Accuracy of satellite sea surface temperatures at 7 and 11 GHz

Chelle L. Gentemann, Thomas Meissner, and Frank J. Wentz

Abstract - Satellite microwave radiometers capable of accurately retrieving sea surface temperature (SST) have provided great advances in oceanographic research. A number of future satellite missions are planned to carry microwave radiometers of various designs and orbits. While it is well-known that the 11 GHz SST retrievals are less accurate than the 7 GHz retrievals, especially in colder waters, it has not been demonstrated using existing microwave data. The Advanced Microwave Scanning Radiometer – Earth Observing System (AMSR-E) provides the means to examine the accuracies of SST retrievals using these channels in a systematic manner. Here, the accuracies of SSTs at 7 and 11 GHz are determined using two approaches: theoretical and empirical. The theoretical accuracies are calculated using an emissivity model and climatology SSTs, while empirical accuracies are estimated through validation of AMSR-E 7 and 11 GHz SST retrievals using over 6 years of data.

I. INTRODUCTION

Sea surface temperatures (SSTs) from satellites carrying microwave radiometers have been continuously available since December 1997 when the Tropical Rainfall Measuring Mission (TRMM) Microwave Imager (TMI) was launched. Microwave 'through-cloud' SST retrievals have become the mainstay for ocean research as they provide an uninterrupted view of the ocean surface, free of cloud and water vapor contamination [1;2]. Areas of active rain do have to be excluded, but they are easily identified and removed. The number of peer-reviewed papers show that microwave SSTs play an important role in earth science research [3-8].

Two National Aeronautics and Space Administration's (NASA) satellite microwave radiometers currently retrieval SST: the previously mentioned TRMM TMI and the Aqua satellite, launched 4 May 2002, carring the Japan Aerospace eXploration Agengy (JAXA) Advanced Microwave Scanning Radiometer – Earth Observing System (AMSR-E) microwave radiometer. TMI is a sun-asynchronous satellite in an equatorial orbit, retrieving data within 40°N-S [9]. It has 9 channels, corresponding to 5 frequencies (11, 19, 24, 37, and 85 GHz) and two polarizations (vertical and horizontal). AMSR-E has 11 channels corresponding to 6 frequencies (7, 11, 19, 24, 37, and 85 GHz) and two polarizations (vertical and horizontal). This is the first polar orbiting microwave radiometer capable of accurate global SSTs since the poorly calibrated Scanning Multi-channel Microwave Radiometer (SMMR) was launched in 1987 [10]. The SST retrieval algorithm used for both TMI and AMSR-E are described in section II.A.

Future radiometers on planned satellite missions are the Global Climate Observation Mission – Weather (GCOM-W) AMSR2 with launch scheduled for February 2011, the Global Precipitation Mission (GPM) Microwave Imager (GMI), with launch scheduled for July 2013, and the National Polar Orbiting Earth System of Systems (NPOESS) Microwave Imager Scanner (MIS) with scheduled launch of 2016. The GCOM-W AMSR2 is an improved AMSR-E, having the same channels as AMSR-E, from 7 - 89 GHz. The GPM GMI is a follow-on to the TRMM TMI, having both a similar sun-asynchronous, high inclination orbit of 60° and channels from 11 - 89 GHz. NPOESS MIS is planned to measure from 7 GHz to 89 GHz (AMSR-E's channels), but will have additional channels at 50, 150, and 183 GHz (used primarily for atmospheric sounding). Since future planned microwave radiometers vary there orbit inclinations and whether

measurements are collected at 7 GHz, it is important to understand the how the accuracy of retrieved SSTs will be impacted.

II. DATA AND ALGORITHM DESCRIPTION

As stated above, the AMSR-E has 11 channels corresponding to 6 frequencies (7, 11, 19, 24, 37, and 85 GHz) and two polarizations (vertical and horizontal). Since May 2002, it has been orbiting at an altitude of 705 km, with a 1.6 m antenna, resulting in a swath width of 1450 km. The AMSR-E data is ideal for examining the accuracy of SSTs from retrieval algorithms using different combinations of the channels.

A. SST RETRIEVAL ALGORITHM

The vertically polarized brightness temperature (T_B) of the ocean surface is sensitive to SST between 4 and 11 GHz [11]. T_B also depends on the sea-surface roughness and on the atmospheric temperature and moisture profile. Fortunately, the spectral and polarimetric signatures of the surface-roughness and the atmosphere are quite distinct from the SST signature, and the influence of these effects can be removed given simultaneous measurements at multiple frequencies and polarizations. Sea-surface roughness, which is tightly correlated with the local wind, is usually parameterized in terms of the near-surface wind speed and direction.

The algorithm regression coefficients are found by generating a large ensemble of simulated T_B computed from a microwave radiative transfer model (RTM) for the ocean and intervening atmosphere [12]. The simulation is based on a set of 42,195 radiosonde soundings launched from weather ships and small islands around the global [13]. These data are used to specify the atmospheric part of the RTM. For each radiosonde, a large range of sea-surface conditions is considered. The sea-surface wind speed is varied from

0 to 40 m s^{-1}, and the wind direction is varied over the full 360° range. The SST is varied by ± 5.5 °C about the Reynolds SST (described in section II.B) for the island site. For each of these Earth scenes, the RTM computes the full set of AMSR-E T_B with realistic sensor noise added. This dataset then consists of known ocean/atmospheric parameters and simulated AMSR-E data.

The AMSR-E SST retrieval algorithm is a physically based regression that expresses SST in terms of T_B. The algorithm operates in two stages. In the first stage, initial estimates of SST and wind speed are obtained via a summation over all the AMSR-E channels using regression coefficients that were determined from a radiative transfer model as is discussed above. The first guess SST provides a reasonable good initial estimate, however, the relationship of T_B versus SST and wind is non-linear, and the simple summation is not capable of fully representing these non-linearities. Hence, we add a second stage to the retrieval algorithm. For the second stage, a large set of localized retrieval algorithms are used. By 'localized', we mean the algorithm is trained to perform well over a relatively narrow range of SST and wind speeds. Localized algorithms are derived for 38 SST reference values ranging from –3 to 34 °C and for 38 wind speed reference values ranging from 0 to 37 m s^{-1}. All SST/wind combinations are considered, thereby giving a total of 1444 localized algorithms. Each algorithm is trained to perform well over a SST/wind range of ±1.5 °C and ±2 m s^{-1} centered on the reference SST and wind value. The reason for using such a large number of algorithms is to ensure good continuity in the retrievals when moving from one set of reference SST/wind to the next. The second-stage retrieval is found from a linear interpolation of the localized algorithms that are in the neighborhood of the first-stage retrievals.

For this study, two SST retrieval algorithms were developed for AMSR-E data, one regression developed using AMSR-E channels 7 – 35 GHz, hereafter referred to as the 7 GHz SST retrieval, and another using AMSR-E channels 11 – 35 GHz, hereafter referred to as the 11 GHz SST retrieval. The first algorithm is identical to the current AMSR-E operational SST algorithm (and future GCOM-W AMSR2), while the second is similar to the TMI operational SST algorithm (and future GPM GMI). The accuracy of these two algorithms was examined using the independent infrared SST data described below.

B. INFRARED SST DATA USED FOR VALIDATION

Two data sets of infrared (IR) SSTs were obtained for validation and are described below. The Reynolds Optimum Interpolated (OI) SST [14] is a weekly global 100 km gridded "bulk" SST analysis produced from satellite and *in situ* SSTs, hereafter referred to as Reynolds SST. The satellite SSTs are from the National Oceanographic Atmospheric Administration (NOAA)'s polar orbiting satellites which carry the Advanced Very High Resolution Radiometer (AVHRR) onboard. SSTs are determined from the AVHRR data using the multi-channel SST algorithm developed by McClain *et al.* [15] and Walton [16]. The static, global, algorithm coefficients are determined through a least-squares regression of the satellite radiances to collocated *in situ* SST measurements. The *in situ* SST measurements used in the Reynolds OI analysis are distributed by the global telecommunication system (GTS) and obtained by volunteer observing ships, drifters, and moored buoys. These *in situ* data are used to correct for any large-scale satellite biases before interpolation of the satellite SSTs. The OI method utilizes estimates of retrieval error, in this application; the nighttime advanced very high resolution radiometer (AVHRR) retrievals are given a smaller error than daytime

retrievals to minimize the impact of any diurnal warming present in daytime retrievals. The analysis is produced in near real-time NRT and is available from 1985 through present. Recently, two additional daily OI SST analyses have been produced by Reynolds, one of which uses the AMSR-E data. The data used here to validation the AMSR-E SST retrievals is the Reynolds weekly analysis that does not include AMSR-E in the analysis.

The Pathfinder (PF) and Erosion monthly climatology [17] is a monthly 9.28 km SST climatology created from the 1985 – 1997 PF AVHRR SSTs. This climatology uses the day and night PF AVHRR SSTs versions 4.0, 4.1, and 4.1 interim. The PF SST algorithm uses a modified nonlinear SST algorithm originally developed by Walton [16]. The modification accounts for temporal sensor calibration drift and errors due to atmospheric water vapor by using two sets of temporally varying algorithm coefficients as described in Evans and Podestá [18]. The climatology was constructed using these SST data, but to maintain the highest quality data, valid SST data adjacent to cloud were excluded. Missing data in the monthly climatology was filled in using Gaussian interpolation. In this study we averaged the monthly 9.28 km climatologies to a single 25 km SST climatology, this data is hereafter referred to as the PF climatology.

III. RETREIVAL ERROR

The total error σ_{total} for a given retrieval algorithm frequency f is

$$\sigma_{total,f} = \sigma_{noise,f} + \sigma_{retrieval,f} + \sigma_{collocation} + \sigma_{data}, \quad (1)$$

where the uncorrelated radiometer noise in each channel results in an error in the retrieved SST, σ_{noise}. This error is non-linear and depends on the earth scene. Errors due to the environmental scene, $\sigma_{retrieval}$, occur because accuracy decreases with increasing

cloud water, wind speed, and water vapor or sub-pixel geophysical variability. When a validation dataset is used, the total error will also include errors due to the collocation $\sigma_{collocation}$ and errors in the independent data set used for validation σ_{data}.

The accuracy of the 7 and 11 GHz SST retrievals are investigated using two methods: theoretical determination of σ_{noise} and empirical errors from validation of actual SST retrievals against independent SST data. Theoretical σ_{noise} is estimated from an emissivity model, where the sensitivity of the brightness temperature to SST is examined. Realistic radiometer noise is added to the brightness temperatures to demonstrate how this impacts errors in SST. Essentially, this method is a theoretical estimate of σ_{noise}. An empirical estimate of σ_{total} is determined from AMSR-E validation results and compare this to the theoretical estimate of σ_{noise}. In the following section we first present the theoretical error followed by comparisons of real-world AMSR-E validation to verify these results.

IV. RESULTS

A. THEORETICAL ESTIMATE OF σ_{noise}

The specular sea surface emissivity E_0 depends on SST, sea surface salinity, and Earth incidence angle. Fig. 1 shows $E_0 \cdot T_S$ (in K), which is the T_B emitted from a specular ocean surface, as function of SST (in °C). The computation was done for vertical and horizontal polarizations at 7.0 GHz and 11.0 GHz, respectively. E_0 was computed from the Fresnel equations [19] using the model for the dielectric constant (permittivity) of sea water by Meissner and Wentz [20], for a Earth incidence equal to that of the AMSR-E instrument, 55°, and a sea surface salinity that is typical of the global

ocean, 35 psu. The sensitivity of T_B to SST illustrated in Fig. 1 is also given in Table 1. The sensitivity is similar above 19 °C but decreases for both channels below 19 °C. The 7 GHz has twice the sensitivity of the 11 GHz channel at 0.0 °C SST. Shibata [21;22] showed similar results using the Klein and Swift dielectric model [23] to determine the sensitivity of SST at 4 and 10 GHz. His results are different due both to the dielectric model and frequencies. The frequencies, given in Table 1, better match existing radiometer configurations. The AMSR-E instrument has noise of 0.1K [12]. Error in SST due to noise is given in Table 2 and shown in Fig. 1 by the horizontal lines. Above 19 ˚C both channels are approximately equally sensitive to SST, but below 19 ˚C the 11 GHz has decreased sensitivity and Fig. 1 shows the increased error by the widening of the horizontal error lines. Table 2 clearly enumerates the differences in errors for the 7 and 11 GHz SST retrievals due to radiometer noise. For 0.1 K noise, the SST error is approximately 0.15 K. The 7 GHz SST error doubles to 0.28 K below -1.0 ˚C. For the 11 GHz channel the error increases, reaching 0.96 K at -1.0 ˚C. These results indicate that at SSTs below 19 ˚C the 7 GHz retrievals will have less error. Table 2 also shows the positive bias at 11 GHz, below 12 °C, introduced by the decreased sensitivity assuming a Gaussian radiometer noise distribution.

The geographical distribution of the theoretical errors was determined using the PF climatology SST dataset (Fig. 2A). The latitudinal region covered by TMI and GMI are shown by red and black lines, respectively. The climatological SSTs range from 15 °C to 28 °C in the region measured by TMI, 40°N-S, and -1 °C to 28 °C in the region measured by GMI, 65°N-S. Fig. 2B shows the theoretical error for the 7 GHz SST retrieval using data from Table 2. Error increases slightly above 40°N-S. Fig. 2C shows the theoretical

error for the 11 GHz SST retrieval. Errors due to radiometer noise increase from 0.16 to 0.43 K at 65°N and 0.87 K at 65°S. The 7 GHz SST retrieval is valid globally while the 11 GHz SST retrieval will have a significant contribution of its error due to radiometer noise above 40°N-S, limiting the usefulness of the data. This effect could be somewhat minimized by using 11 GHz SST data averaged into weekly or monthly maps where the uncorrelated errors due to radiometer noise would be diminished, but this will also minimize it's usefulness for research requiring sub-weekly or monthly variability which can be significant.

B. EMPIRICAL ESTIMATE OF σ_{noise}

To examine whether the errors due to decreased sensitivity in the 11 GHz channel are visible in actual SST retrievals, we used Reynolds SSTs linearly interpolated in time and space to match the AMSR-E data which was processed using both the 7 and 11 GHz SST retrieval algorithms. Identical rain, sun glitter, and side-lobe contamination flags were used to exclude data for both SST retrieval algorithms. Collocated data from 1 June 1 2002 – 31 December 2008 were used to determine SST error.

The global standard deviation of AMSR-E minus Reynolds SST is shown in Fig. 3. Similar to Fig. 2, the TMI and GMI measurement areas are shown both on the left of the Fig. and by lines at the corresponding latitudes. The right panel shows the mean error by latitude. As discussed previously, the error calculated in this manner will include error due to radiometer noise, retrieval error, collocation error, and errors in the Reynolds SST. The comparison between a 25 km satellite SST retrieval and the 100 km weekly averaged Reynolds has a collocation error $\sigma_{collocation}$. If we assume that $\sigma_{collocation}$ can be approximated by a single number, we can estimate $\sigma_{collocation}$ by forcing the difference in

the theoretical error and empirical error in tropical regions, where σ_{noise} is minimal, to be zero. Fig. 3A and 3B both show the assumed $\sigma_{collocation}$, in the lower left corner of each panel.

The 7 GHz retrievals (Fig. 3A) show the least error in the tropics, increasing towards the polar regions. Error due to σ_{data} is visible in the Kuroshio, Gulf Stream, Agulhas, and Brazil-Malvinas confluence regions. These currents are temporally and spatially highly variable and are not well resolved by the low temporal and spatial resolution of the Reynolds analysis used for comparison. The 11 GHz (Fig. 3B) and 7 GHz errors have a similar magnitude and spatial structure in the tropical regions, but above 40°N-S the error increases significantly in the 11 GHz retrievals.

The latitudinal average errors for the data (Fig. 4A) and the model using climatological SST (Fig. 4B) clearly show the increase in error above 40°N-S for the 11 GHz retrievals. The data shows an increase in error in both the 7 and 11 GHz retrievals at approximately 40°N-S, but Fig. 3 demonstrated that this effect is due to the western boundary currents. Generally, the data show that the retrievals have similar error at latitudes < 40°N-S, but the 11 GHz increases significantly at higher latitudes. The sensitivity model using PF climatology SST (Fig. 4B) does not show the strong increase at the latitudes of the western boundary currents since the error only depends on SST, not collocations of SST. The model shows similar errors at latitudes less than 40°N-S and the 11 GHz error increases quickly above 40°N-S. Unlike the data, the model does not show a reduction in error at the highest latitudes. To further explore this, Fig. 4C shows $\sigma_{noise,11}$ (red) from the theoretical estimate. To compare the theoretical and empirical $\sigma_{noise,11}$, we remove the errors due to collocation and errors in the Reynolds data as

follows. Using Equation (1), we take the difference empirical 11 GHz errors minus empirical 7 GHz error plus $\sigma_{noise,7}$ to find

$$\underbrace{\sigma_{total,11} - \sigma_{total,7}}_{empirical} + \underbrace{\sigma_{noise,7}}_{theoretical} = \underbrace{\sigma_{noise,11} + \underbrace{(\sigma_{retrieval,11} - \sigma_{retrieval,7})}_{positive}}_{B} \quad (2)$$

$\sigma_{total,11}$ and $\sigma_{total,7}$ are given by the validation results and $\sigma_{noise,7}$ was determined theoretically. Therefore, the green line *B* is the 11 GHz SST error due to noise plus the difference in retrieval error, which should usually be positive because the 11 GHz SST retrieval is less accurate, especially in colder waters. Therefore, as expected, the theoretical estimated and *B*, in Fig. 4C, are similar in the tropics where there are warmer temperatures. The error *B* is larger from 40-60°S and 40-70°N due to an increase in 11 GHz retrieval error for cold water. Polewards, *B* decreases and is less than the theoretical estimate of $\sigma_{noise,11}$.

The decrease in error at the highest latitudes is explained by Fig. 5. The probability density function (PDF) of the collocation error (background color), mean bias (solid line), and standard deviation (dashed lines) for the 7 GHz (Fig. 5A) and 11 GHz (Fig. 5B) show the dramatic increase in error for the 11 GHz retrieval below 12 °C. The STD as a function of SST (Fig. 5C) also shows the dramatic increase. The AMSR-E data minimum value is -1.8 °C. At 7 °C the number of large positive differences steadily decreases because of the -1.8 °C minimum temperature. The largest differences are about 7.5 °C, so at 7 °C, AMSR-E can either be 14.5 °C larger or -0.5 °C smaller than the 7 °C Reynolds. Below 7 °C, AMSR-E cannot be less than -1.8 °C, so the bias magnitude increases while the error appears to decrease. This explains the reduction at high latitudes seen in Fig. 3 and Fig. 4.

Finally, the larger error seen at the mid-latitudes in Fig. 4, attributed to retrieval error, is demonstrated in Fig. 6. The 7 GHz SST (Fig. 6A) is clearly less noisy than the 11 GHz SST (Fig. 6B). There is a visible 'swirl' feature south of Alaska in the 11 GHz SST that is less obvious in the 7 GHz SST. This feature can be seen in the AMSR-E water vapor (Fig. 6C) and the difference (7 minus 11 GHz) SSTs. The 11 GHz SST retrieval is not performing as well as the 7 GHz retrieval over cold water with varying water vapor. These water vapor features are common from 40-60°N-S, in both hemispheres and may account for the increased error seen in Fig. 5.

V. CONCLUSIONS

The 7 GHz SST retrievals have less errors due to radiometer noise and geophysical errors than the 11 GHz retrievals at all latitudes. The error for the 11 GHz SST retrieval increases polewards of 40°N-S. Although the addition of a 7 GHz feedhorn to a radiometer is costly, the polar regions are increasingly important areas to monitor for environmental changes and the use of 7 GHz would provide more accurate data. Additionally, while averaging the 11 GHz will diminish error due to uncorrelated radiometer noise, the geophysical error is still higher than 7 GHz retrievals, especially at the higher latitudes. The success of the TRMM TMI microwave SST retrievals is partly due to its limited orbit, measuring between 40°N-S and the GPM GMI will have larger errors with its expanded orbit measuring between 65°N-S.

V1. ACKNOWLEDGEMENTS

The Pathfinder Erosion Climatology was downloaded from NASA's Physical Oceanography Distributed Active Archive Center (PO.DAAC). The Reynolds Optimum Interpolation SST v2 were downloaded from NOAA's National Weather Service (NWS)

Environmental Modeling Center (EMC). The AMSR-E SSTs are from Remote Sensing Systems, processed using the version 5 algorithm, and available at www.remss.com. This work was funded by the NASA Physical Oceanography program manager, Eric Lindstrom, grant NNH08CC60C.

V11. FIGURES

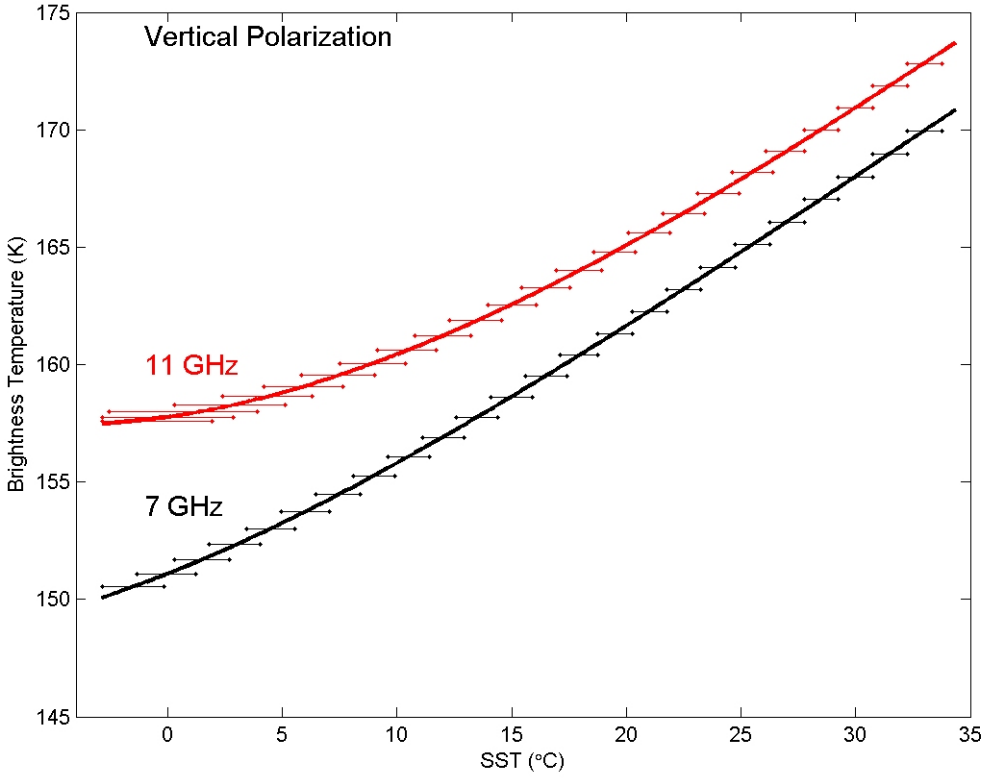

Fig. 1. Relationship between 7 and 11 GHz (vertical polararization) and SST. The horizontal lines show the error in SST due to 0.5K noise in brightness temperature. Actual noise is 0.1 K, but this larger noise value was used to better illustrate the increase in error. The sensitivity of SST to changes in TB decreases for the 11 GHz at lower SSTs, resulting in larger errors and a small positive bias (Table 2).

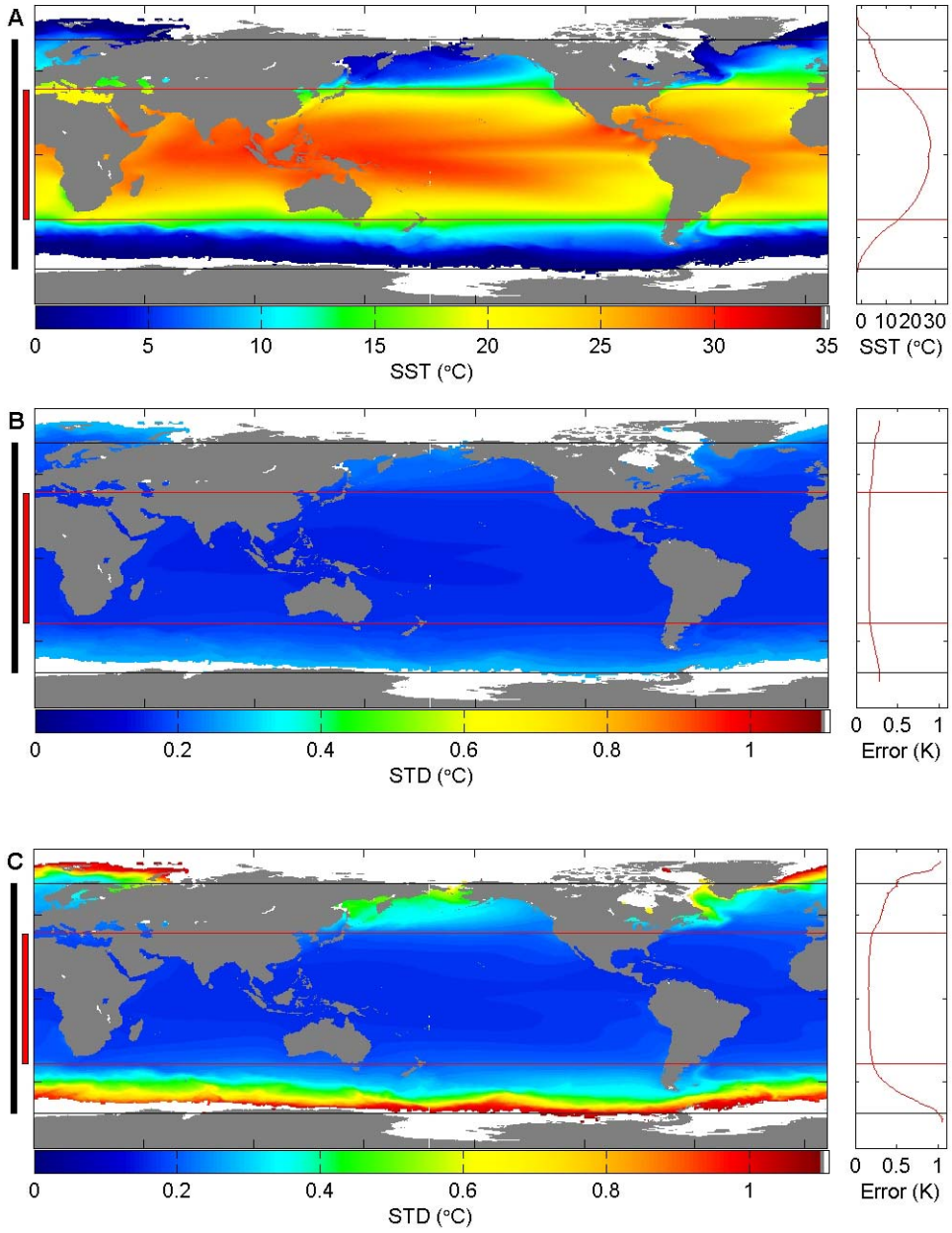

Fig. 2. Sensitivity of SST error due to radiometer noise. The latitudes measured by TMI (red) and GMI (black) are shown on the left side of each panel. The latitudinal average is shown to the right of the panels. Panel A) PF Climatology SST. Panel B) Noise error for SST retrievals at 7 GHz. Panel C) Noise error for SST retrievals using 11 GHz. Above 40°N-S, the SST retrievals will have increased error due to the decreased sensitivity.

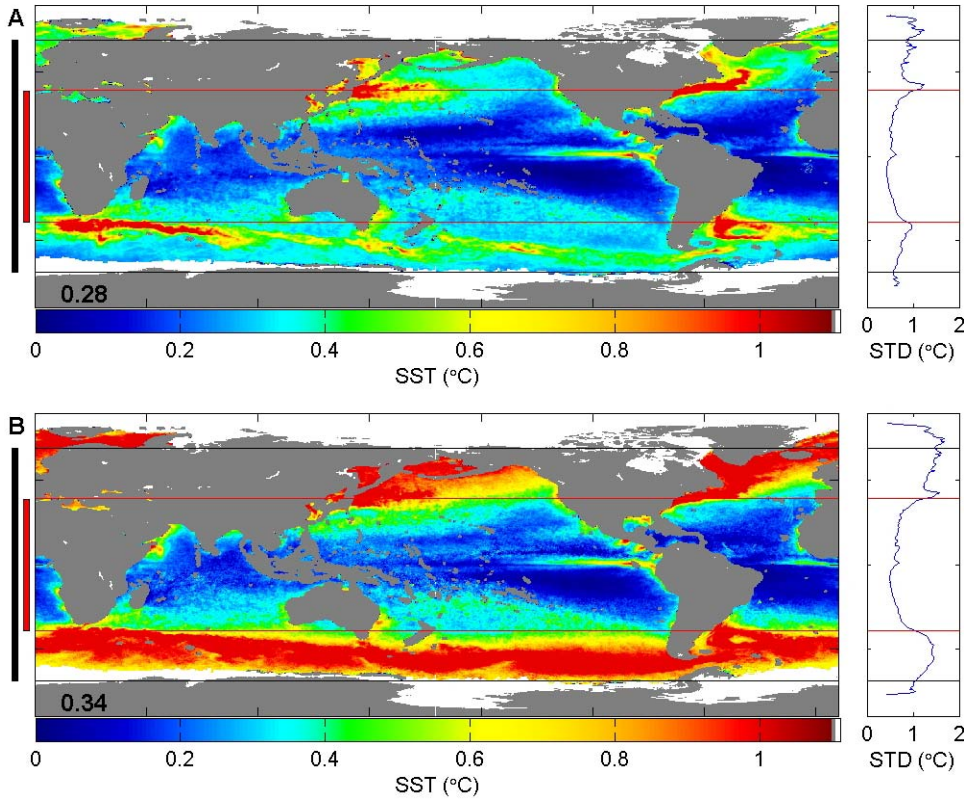

Fig. 3. The standard deviation of AMSR-E minus Reynolds SST for the (A) 7 GHz AMSR-E SSTs and (B) 11 GHz AMSR-E SSTs. The latitudes measured by TMI (red) and GMI (black) are shown on the left side of each panel. The latitudinal average is shown to the right of panels. An estimate of the collocation error, given in the lower left corner, was subtracted from each image.

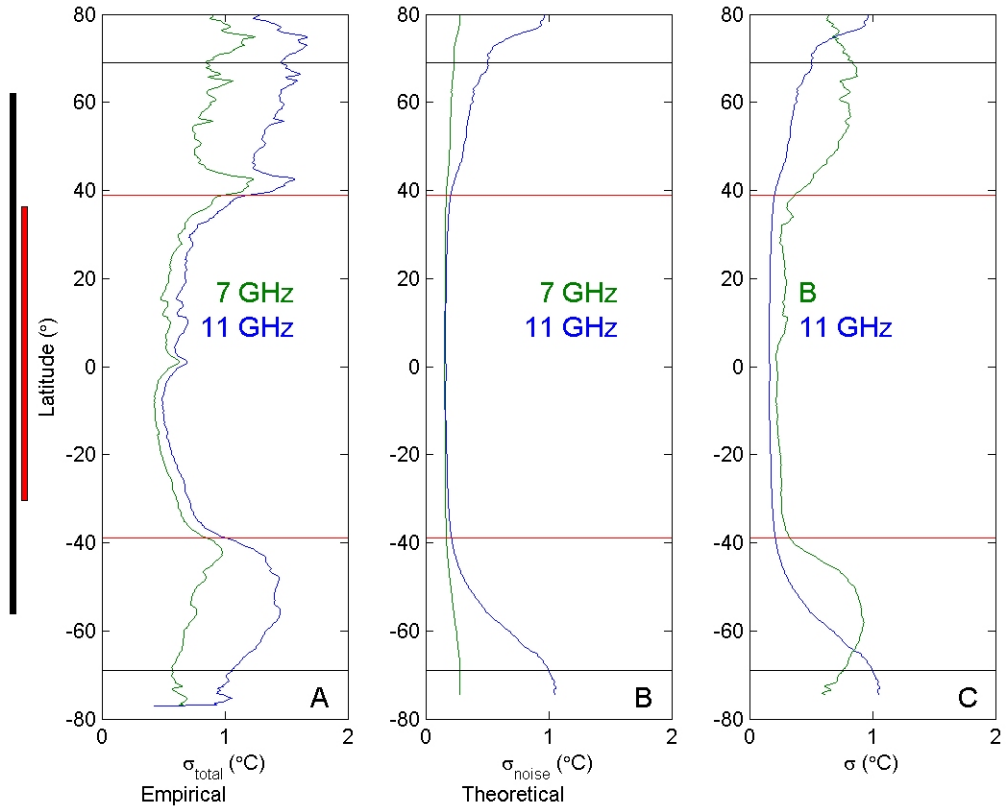

Fig. 4. Latitudinal average standard deviation for (A) Data (AMSR-E minus Reynolds SST), (B) Model (error from Table 2 and climatology SST), (C) 11 GHz model (red) and 11 GHz minus 7 GHz data error. The latitudes measured by TMI (red) and GMI (black) are shown on the left side of each panel.

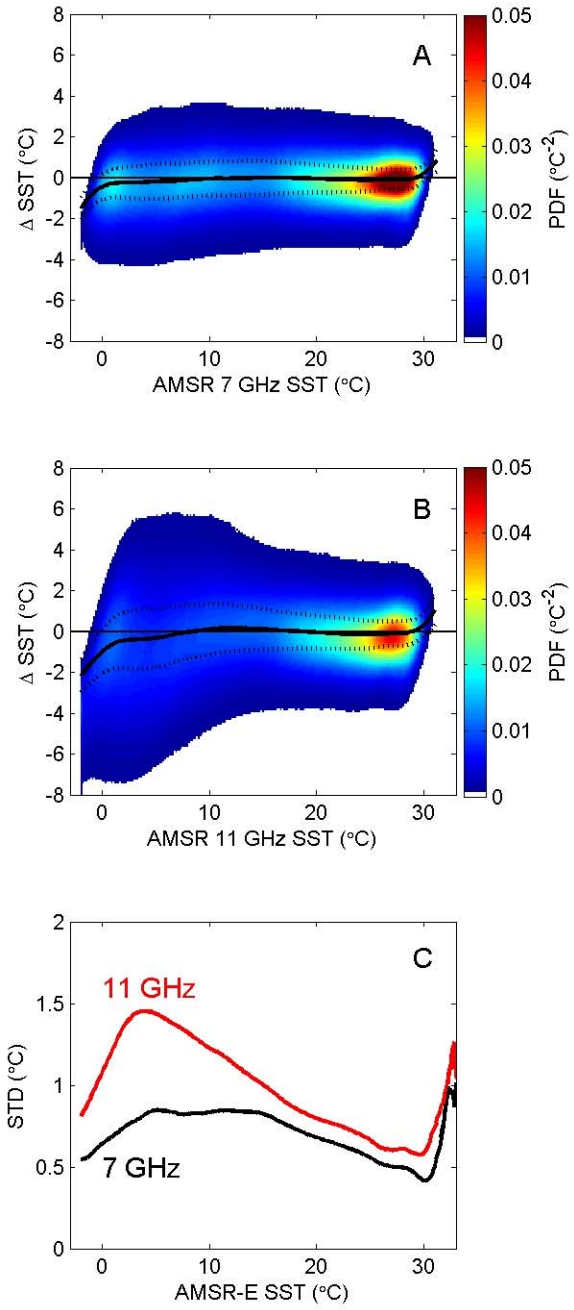

Fig. 5. AMSR-E minus Reynolds SST, ΔSST, as a function of AMSR-E (A) 7 GHz SST, (B) 11 GHz SST, and (C) the standard deviation of ΔSST as a function of AMSR-E SST.

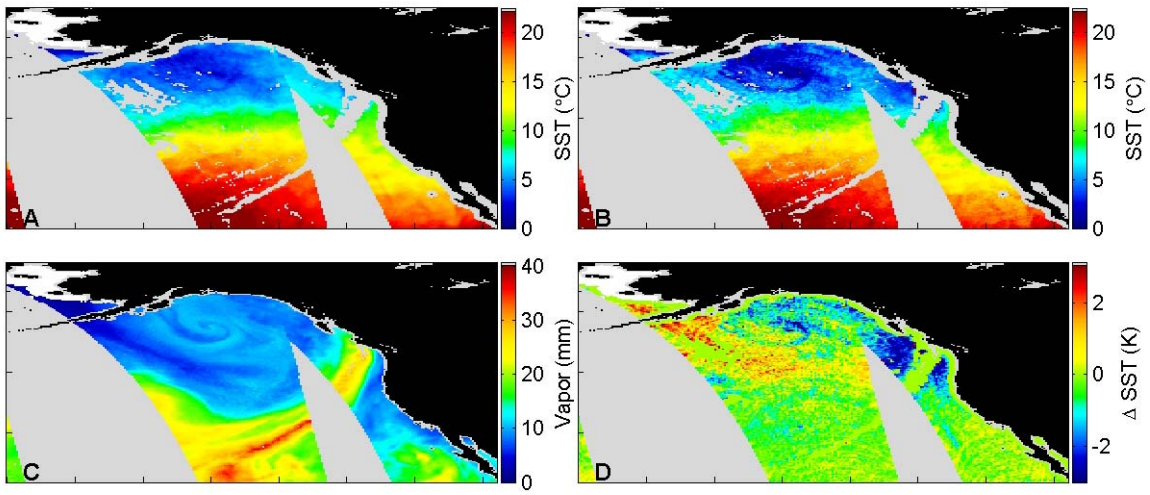

Fig. 6. 1 January 2008 AMSR-E retrievals of (A) 7 GHz SST, (B) 11 GHz SST, (C) Water Vapor, and (D) 11 GHz minus 7 GHz SSTs.

V111. Tables

Table 1. Sensitivity of 7 and 11 GHz vertical polarization measurements to SST

SST (°C)	Sensitivity to SST (K °C^{-1})	
	7 GHz	11 GHz
0.00	0.39	0.14
15.00	0.59	0.47
30.00	0.65	0.63

Table 2. The error in SST due to a 0.1 K noise in brightness temperature at 7 and 11 GHz (vertical polarization). The errors are approximately equal above 19 °C, but below that, the 11 GHz error is always larger than the 7 GHz error, increasing from 0.20 to 0.96 ˚C.

SST (°C)	SST STD error		SST bias	
	7 GHz	11 GHz	7 GHz	11 GHz
-1.00	0.28	0.96	0.00	0.13
0.00	0.26	0.75	0.00	0.09
1.00	0.25	0.61	0.00	0.05
2.00	0.24	0.53	0.00	0.04
3.00	0.23	0.46	0.00	0.03
4.00	0.22	0.41	0.00	0.02
5.00	0.21	0.37	0.00	0.02
6.00	0.20	0.34	0.00	0.02
7.00	0.20	0.31	0.00	0.02
8.00	0.19	0.30	0.00	0.01
9.00	0.19	0.28	0.00	0.01
10.00	0.18	0.27	0.00	0.01
11.00	0.18	0.26	0.00	0.01
12.00	0.18	0.24	0.00	0.01
13.00	0.18	0.23	0.00	0.00
14.00	0.17	0.22	0.00	0.00
15.00	0.17	0.22	0.00	0.00
16.00	0.17	0.20	0.00	0.00
17.00	0.17	0.20	0.00	0.00
18.00	0.16	0.20	0.00	0.00
19.00	0.16	0.19	0.00	0.00
20.00	0.16	0.19	0.00	0.00
21.00	0.16	0.18	0.00	0.00
22.00	0.16	0.18	0.00	0.00
23.00	0.16	0.18	0.00	0.00
24.00	0.16	0.17	0.00	0.00
25.00	0.16	0.17	0.00	0.00
26.00	0.16	0.17	0.00	0.00
27.00	0.16	0.16	0.00	0.00
28.00	0.15	0.16	0.00	0.00
29.00	0.15	0.16	0.00	0.00
30.00	0.15	0.16	0.00	0.00
31.00	0.15	0.16	0.00	0.00
32.00	0.15	0.16	0.00	0.00
33.00	0.15	0.16	0.00	0.00
34.00	0.15	0.16	0.00	0.00

IX. References

[1] D. B. Chelton and F. J. Wentz, "Global microwave satellite observations of sea surface temperature for numerical weather prediction and climate research," *Bulletin of the American Meteorological Society*, vol. 86, no. 8, pp. 1097-1115, 2005.

[2] F. J. Wentz, C. L. Gentemann, D. K. Smith, and D. B. Chelton, "Satellite measurements of sea surface temperature through clouds," *Science*, vol. 288, no. 5467, pp. 847-850, 2000.

[3] D. B. Chelton, F. J. Wentz, C. L. Gentemann, R. A. D. Szoeke, and M. G. Schlax, "Satellite microwave SST observations of transequatorial tropical instability waves," *Geophysical Research Letters*, vol. 27, no. 9, pp. 1239-1242, 2000.

[4] D. B. Chelton, S. K. Esbensen, M. G. Schlax, N. Thum, M. H. Freilich, F. J. Wentz, C. L. Gentemann, M. J. McPhaden, and P. S. Schopf, "Observations of coupling between surface wind stress and sea surface temperature in the eastern tropical Pacific," *Journal of Climate*, vol. 14, no. 7, pp. 1479-1498, 2001.

[5] C. J. Donlon, C. L. Gentemann, and F. J. Wentz, "Measuring surface temperature with microwave sensors," *Backscatter*, vol. 12, pp. 37-39, 2001.

[6] C. L. Gentemann, P. J. Minnett, P. Le Borgne, and C. J. Merchant, "Multi-satellite measurements of large diurnal warming events," *Geophysical Research Letters*, vol. 35, no. L22602 2008.

[7] R. W. Reynolds, C. L. Gentemann, and F. J. Wentz, "Impact of TRMM SSTs on a climate-scale SST analysis," *Journal of Climate*, vol. 17, no. 8, pp. 2938-2952, 2004.

[8] D. Stammer, F. J. Wentz, and C. L. Gentemann, "Validation of microwave sea surface temperature measurements for climate purposes," *Journal of Climate*, vol. 16, no. 1, pp. 73-87, 2003.

[9] C. D. Kummerow, W. Barnes, T. Kozu, J. Shieu, and J. J. Simpson, "The tropical rainfall measuring mission (TRMM) sensor package," *Journal of Atmospheric and Oceanic Technology*, vol. 15, no. 3, pp. 809-817, 1998.

[10] F. J. Wentz, C. L. Gentemann, D. K. Smith, and D. B. Chelton, "Satellite measurements of sea surface temperature through clouds," *Science*, vol. 288, no. 5467, pp. 847-850, 2000.

[11] J. P. Hollinger and R. C. Lo, "Determination of sea surface temperature with N-ROSS," Naval Research Laboratory, Naval Research Laboratory Memorandum Report 5375 5375, 1984.

[12] F. J. Wentz and T. Meissner, "AMSR Ocean Algorithm, Version 2,", 121599A-1 ed Santa Rosa, CA: Remote Sensing Systems, 2000, p. 66.

[13] F. J. Wentz, "A well calibrated ocean algorithm for special sensor microwave / imager," *Journal of Geophysical Research*, vol. 102, no. C4, pp. 8703-8718, 1997.

[14] R. W. Reynolds and T. M. Smith, "Improved global sea surface temperature analyses using optimum interpolation," *Journal of Climate*, vol. 7, pp. 929-948, 1994.

[15] E. P. McClain, W. G. Pichel, and C. C. Walton, "Theory and validation of the multiple window sea surface temperature technique," *Journal of Geophysical Research*, vol. 90, pp. 11587-11601, 1985.

[16] C. C. Walton, "Nonlinear multichannel algorithms for estimating sea surface temperature with AVHRR satellite data," *Journal of Applied Meteorology*, vol. 27, pp. 115-124, 1988.

[17] K. S. Casey and P. Cornillon, "A comparison of satellite and *in situ*-based sea surface temperature climatologies," *Journal of Climate*, vol. 12, pp. 1848-1863, 1999.

[18] R. Evans and G. P. Podestá, "Pathfinder sea surface temperature algorithm version 4.0," RSMAS U. Miami, Miami,1998.

[19] J. D. Jackson, *Classical Electrodynamics*, 3rd ed. New York: Wiley, 1975, p. 832.

[20] T. Meissner and F. J. Wentz, "The complex dielectric constant of pure and sea water from microwave satellite observations," *IEEE Transactions on Geoscience and Remote Sensing*, vol. 42, no. 9, pp. 1836-1849, 2004.

[21] A. Shibata, "Calibration of AMSR-E SST toward a monitoring of global warming,", 5 ed Seoul, Korea: 2005, pp. 3448-3449.

[22] A. Shibata, "Features of ocean microwave emission changed by wind at 6 GHz," *Journal of Oceanography*, vol. 62, pp. 321-330, 2006.

[23] L. A. Klein and C. T. Swift, "An improved model for the dielectric constant of sea water at microwave frequencies," *IEEE Transactions on Antennas and Propagation*, vol. AP-25, pp. 104-111, 1977.